ARTICLE NO. 79-0139R

J80-170

Pseudo-Direct Solution to the Boundary-Layer Equations for Separated Flow

20005
20007

Rimon Arieli* and John D. Murphy†
NASA Ames Research Center, Moffett Field, Calif.

This paper describes a procedure for the automatic iteration of an inverse boundary-layer technique to a prescribed pressure distribution in a separated flow. The technique is demonstrated by using the pressure distributions from two transonic airfoil flows and two externally generated shock-wave/boundary-layer interactions as objective functions of an optimization loop driving an inverse boundary-layer code. The skin friction and wake centerline velocity distributions computed as a part of the solutions are compared to experimental data and to solutions of full Navier-Stokes equations. These comparisons indicate that substantial economies can be obtained by applying methods like the present, in lieu of full Navier-Stokes methods, in zonal calculation schemes for design purposes. The optimization technique leading to convergence is described in detail and a table of typical computation time is presented.

Nomenclature

$\bar{A}$ = matrix of sensitivity derivatives
C_f = skin-friction coefficient, $\tau_w/(1/2)\rho_e u_e^2$
C_p = pressure coefficient, $2/\gamma M_\infty^2 (P_e/P-1)$
C = Chapman-Rubesin constant
DC = difference coefficient multiplying terms at x station
DM = difference coefficient multiplying terms at $x-\Delta x$ station
DP = difference coefficient multiplying terms at $x+\Delta x$ station
f = dimensionless stream function
h = static enthalpy
K = number of stations in the separated flow region
K_1 = coefficient $\sqrt{2\xi/\rho_e\mu_e}$
ℓ = mixing length
N = number of nodes in y direction
$\bar{P}$ = vector of external pressure ratio
p = pressure
R = gas constant
T = temperature
u = velocity component in x direction
v = velocity component in y direction
x = streamwise coordinate
y = cross-stream coordinate
α = angle of attack
β = boundary-layer pressure-gradient parameter, $(2\xi/u_e)(du_e/d\xi)$
γ = ratio of specific heat
δ = boundary-layer thickness
δ^* = displacement thickness
η = transformed normal coordinate
η_{edge} = value of η at boundary-layer edge
μ = viscosity
ξ = transformed longitudinal coordinate
ρ = density
$\bar{\sigma}$ = vector of prescribed boundary condition in the separated flow
σ = prescribed boundary condition
τ = shear stress
τ_T = turbulent shear stress

Subscripts

e = boundary-layer edge
i = ith x point
j = jth y point
k = kth x point in the separation bubble
w = wall conditions

Superscripts

m = iteration number
0 = nominal value

Introduction

IT is commonly agreed that the problem of separating and reattaching flows is one of the most difficult problems in computational fluid dynamics. The need for accurate prediction of flows containing such regions has been further emphasized recently by the increased interest in transonic flight. It is also generally accepted that the Navier-Stokes equations provide the best mathematical description of the complete flowfield including separation regions. It has been shown,[1-3] however, that for thin-shear layers containing slender separation bubbles, the boundary-layer equations provide an adequate description of the flow at far less cost than Navier-Stokes calculations of comparable accuracy. In addition to the large amount of computing time required by Navier-Stokes solutions, storage capabilities on present computers limit flowfield resolution when practical problems are considered. As a result of the need for flow solutions about practical, complex geometries at reasonable cost, the advantage of solutions using boundary-layer-type approximations should not be overlooked. A detailed summation of the status of Navier-Stokes solvers is contained in Ref. 4.

Substantial progress has been made since Catherall and Mangler in 1966 in the integration of the boundary-layer equations through the saddle-type singularity at the separation point. This has been accomplished by specifying either the displacement thickness or skin friction, $\delta^*(x)$ or $C_f(x)$, and computing the pressure distribution $p(x)$ as part of the solution, i.e., inverse calculations. There are, however, substantial practical disadvantages to inverse calculations if the coupling to the inviscid flow is neglected, since one must

Presented as Paper 79-0139 at the AIAA 17th Aerospace Sciences Meeting, New Orleans, La., Jan. 15-17, 1979; submitted Feb. 15, 1979; revision received Jan. 10, 1980. This paper is declared a work of the U.S. Government and therefore is in the public domain.

Index categories: Computational Methods; Jets, Wakes, and Viscid-Inviscid Flow Interactions.

*National Research Council Research Associate. Member AIAA.
†Research Scientist.

specify, as a boundary condition, the ab initio unknown distribution of a parameter of the solution. The appropriateness of the distribution used is then determined by matching to experimental data or to an outer flow solution. Generally, the assumed boundary-layer parameter will not lead to the external pressure distribution desired, and an iteration procedure is required by which successive alterations are made in the first guess of $\delta^*(x)$ or $C_f(x)$ until the "correct" solution is obtained. Such "manual" iteration techniques have been based largely on a cut-and-try procedure, a tedious task that relies heavily on the user's experience and judgment.

In this paper, a fully automated procedure which permits the calculation of solutions to the boundary-layer equations for a specified pressure distribution in the presence of a separation bubble is described. Although the optimization concept is not limited to producing a desired pressure distribution, the authors have not yet attempted to implement the concept in connection with other parameters. This work arises from the motivation to develop economical, simple to use, and reasonably accurate engineering calculations for flowfields containing separation regions. The computational results, along with typical computational times, demonstrate that the technique is a significant improvement in the method of treating separated flows.

Analysis

The present method is composed of two parts: the solution of the boundary-layer equations referred to as the basic solution, and a technique to correctly modify the assumed boundary conditions to meet the desired pressure variation.

Boundary-Layer Solution

The boundary-layer equations are solved in either an inverse or direct mode, using the generalized Galerkin method.[5,6] The equations considered are:

Continuity:

$$\frac{\partial \rho u}{\partial x}+\frac{\partial \rho v}{\partial y}=0 \tag{1}$$

Momentum:

$$\rho u\frac{\partial u}{\partial x}+\rho v\frac{\partial u}{\partial y}=-\frac{\mathrm{d}p}{\mathrm{d}x}+\frac{\partial}{\partial y}\left(\mu\frac{\partial u}{\partial y}+\rho\tau_T\right) \tag{2}$$

Energy:

$$h+(u^2/2)=\text{constant} \tag{3}$$

State:

$$p=\rho RT \tag{4}$$

where turbulent shear

$$\rho\tau_T=\rho\ell^2\left|\frac{\partial u}{\partial y}\right|\frac{\partial u}{\partial y}$$

As commonly used in boundary-layer solutions, the Levy-Lees-Dorodnitsyn transformation is applied to permit the computational domain to grow in the streamwise direction, following to some extent the growth of the boundary layer. By doing so, the physical plane (x,y) is mapped into a computational domain (ξ,η)

$$\xi(x)=\int_0^x \rho_e u_e \mu_e \mathrm{d}x$$

$$\eta(x,y)=\frac{\rho_e u_e}{\sqrt{2\xi}}\int_0^y \frac{\rho}{\rho_e}\mathrm{d}y \tag{5}$$

Defining a stream function

$$f(\xi,\eta)=\frac{1}{\sqrt{2\xi}}\int_0^y \rho u\mathrm{d}y$$

the first derivative with respect to η becomes the nondimensional longitudinal velocity u/u_e. The continuity equation when combined with the momentum equation and rewritten in stream-function variables results in the well-known boundary-layer equation

$$\frac{\partial}{\partial\eta}Cf_{\eta\eta}+ff_{\eta\eta}+\beta\left(\frac{1}{\bar\rho}-f_\eta^2\right)+K_1\frac{\partial}{\partial\eta}\bar\rho\tau_T=2\xi\left(f_\eta f_{\eta\xi}-f_{\eta\eta}f_\xi\right) \tag{6}$$

When using the generalized Galerkin method, approximate functions for the dependent variables must be provided. Following the technique of Ref. 3, the stream function (f), the velocity (f_η), and the shear $(f_{\eta\eta})$ are approximated by Taylor series between adjacent mesh points in the η direction, assuming a constant fourth derivative $(f_{\eta\eta\eta\eta})$ across the interval (η_i,η_{i+1}).

Figure 1 shows a schematic representation of the typical flow regimes characterizing a separated reattaching flow. The point of this figure is to illustrate the type-dependent streamwise difference modules used in the several regions. The streamwise derivatives are approximated by forward, backward, or central differencing, depending on the local value of f_η, using the following general difference equation:

$$(f_\xi)_{i,j}=DPf_{i+1,j}+DCf_{i,j}+DMf_{i-1,j} \tag{7a}$$

At nodal points where the local velocity is in the mainstream direction, $f_\eta>0.01$ backward differences are used where:

$$DP=0,\quad DM=\frac{-2}{\ell n(\xi_i/\xi_{i-1})},\quad DC=\frac{2}{\ell n(\xi_i/\xi_{i-1})} \tag{7b}$$

Near the zero-velocity line, $-0.01\le f_\eta\le 0.01$, central differences are used where:

$$DP=\frac{1-100f_\eta}{\ell n\xi_{i+1}/\xi_i},\quad DM=-\frac{(1+100f_\eta)}{\ell n\xi_i/\xi_{i-1}},$$

$$DC=-(DM+DP) \tag{7c}$$

When the flow is reversed, $f\le -0.01$, forward differencing is used with the following coefficients:

$$DP=\frac{2}{\ell n(\xi_{i+1}/\xi_i)},\quad DC=\frac{-2}{\ell n(\xi_{i+1}/\xi_i)} \tag{7d}$$

Note that in the region of reversed flow, $x_{\text{sep}}\le x\le x_{\text{reattach}}$, the equations are not strictly elliptic but rather parabolic in opposite directions. That is to say the relevant characteristic line points downstream for $u>0$ while it points upstream for $u<0$. This condition imposes the need for iterative sweeping as a solution technique if one wishes to avoid the additional approximation of ignoring convection in the region of backflow. The type-dependent differencing used in this region properly accounts for this change in characteristic direction, while leaving the strictly downstream parabolic regions unchanged.

The boundary-layer equation is then integrated with respect to a unit square-wave weighting function from η_j to η_{j+1} resulting in a momentum equation for the strip (η_j,η_{j+1}).[3] The set of equations contains $N-1$ nonlinear algebraic momentum equations, where N is the number of nodal points normal to the surface. The Taylor series expansions for the η derivatives provide a sequence of $3(N-1)$ additional linear

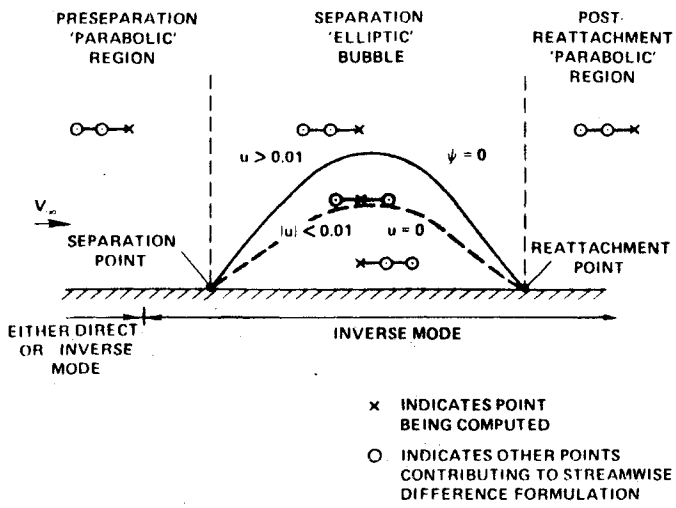

Fig. 1 Schematic of streamwise division of computational domain.

algebraic equations. The remaining four equations are imposed as boundary conditions.

For attached flow these equations are solved in the direct mode (i.e., $\beta(x)$ known) and the boundary conditions are

$$\text{at} \quad \eta=0 \qquad f=f_\eta=0$$

$$\text{at} \quad \eta=\eta_{\text{edge}} \qquad f_\eta=1, \quad f_{\eta\eta}=0 \tag{8a}$$

For separated flow the equations are solved in the inverse mode, and $\beta(x)$ is computed as part of the solution subject to the boundary conditions:

$$\left.\begin{aligned} &\text{at} \quad \eta=\eta_{\text{edge}} \quad f_\eta=1, \quad f_{\eta\eta}=0\\ &\text{at} \quad \eta=0 \quad f=0\\ &\qquad\qquad f_\eta=0\\ &\qquad\qquad f_{\eta\eta}=\sigma_\tau(\xi)\\ &\text{or} \quad\quad f=0\\ &\qquad\qquad f_\eta=\sigma_u(\xi)\\ &\qquad\qquad f_{\eta\eta}=0 \end{aligned}\right\} \tag{8b}$$

where σ_τ is the shear stress at the wall and σ_u is the wake centerline velocity. Note that in the latter case the system of equations is overdetermined if $\beta(\xi)$ is specified. We avoid this difficulty by treating $\beta(\xi)$ as the free parameter which is determined as a part of the solution. Actually, $\beta(\xi)$ is computed using the momentum equation integrated over the first strip.

The solution procedure has been modified since the presentation of the paper in January 1979. At present, the system of $4N$ algebraic equations is cast in block tridiagonal form and solved by $L-U$ decomposition. This provides nearly an additional factor of ten in speed over the original computer code.

Correction Loop

When the boundary-layer equations are solved in the inverse mode, an additional boundary condition is prescribed. In general, such a solution will not meet the desired pressure distribution and a correction loop is needed. In the present method, the correction loop is based on a Newton-Raphson iteration procedure. We expand the pressure as a Taylor series in terms of the additional boundary condition.

$$p^{m+1}(x)=p^m(x)+(\partial p/\partial\sigma)^m\Delta\sigma+0(\Delta\sigma)^2 \tag{9}$$

Where $p^{m+1}(x)$ can be identified with the desired pressure distribution, and $p^m(x)$ is the pressure distribution as computed at the mth iteration. The incremental change in σ required to force the inverse boundary-layer solution in the direction of the desired pressure is given by

$$\Delta\sigma=\frac{p^{m+1}(x)-p^m(x)}{(\partial p/\partial\sigma)^m} \tag{10}$$

The solution of this equation for $\Delta\sigma$ can be obtained provided that the partial derivative of $p(x)$ with respect to σ is known or can be evaluated at each x location. This partial derivative, i.e., "the sensitivity function," is evaluated by solving a set of perturbation equations. These equations are obtained by differentiating the boundary-layer equation, the Taylor series expansions, and the boundary conditions with respect to σ.[7,8] The perturbation of the Taylor expansions are:

$$(f_\sigma)_{j+1}=(f_\sigma)_j+(f_{\eta\sigma})_j\Delta\eta+(f_{\eta\eta\sigma})_j\frac{\Delta\eta^2}{2}+(f_{\eta\eta\eta\sigma})_j\frac{\Delta\eta^3}{3}+(f_{\eta\eta\eta\sigma})_{j+1}\frac{\Delta\eta^3}{24} \tag{11a}$$

$$(f_{\eta\sigma})_{j+1}=(f_{\eta\sigma})_j)+(f_{\eta\eta\sigma})_j\Delta\eta+(f_{\eta\eta\eta\sigma})_j\frac{\Delta\eta^2}{3}+(f_{\eta\eta\eta\sigma})_{j+1}\frac{\Delta\eta^2}{6} \tag{11b}$$

$$(f_{\eta\eta\sigma})_{j+1}=(f_{\eta\eta\sigma})_j+(f_{\eta\eta\eta\sigma})_j\frac{\Delta\eta}{2}+(f_{\eta\eta\eta\sigma})_{j+1}\frac{\Delta\eta}{2} \tag{11c}$$

The perturbed-momentum equation is:

$$\begin{aligned}&(C_\sigma f_{\eta\eta}+Cf_{\eta\eta\sigma})_\eta+(ff_{\eta\eta\sigma}+f_\sigma f_{\eta\eta})+\beta\left[\left(\frac{1}{\bar\rho}\right)_\sigma-2f_\eta f_{\eta\sigma}\right]\\&+\beta_\sigma\left(\frac{1}{\bar\rho}-f_\eta^2\right)+K_1(\rho\tau_T)_\sigma\\&=2\xi(f_\eta f_{\eta\xi\sigma}+f_{\eta\sigma}f_{\eta\xi}-f_{\eta\eta}f_{\xi\sigma}-f_{\eta\eta\sigma}f_\xi)\end{aligned} \tag{12}$$

The streamwise derivatives are treated in a way similar to the basic solution. The boundary conditions for these equations are

$$\text{at} \quad \eta=0 \qquad f_\sigma=0$$

$$\text{and} \quad f_{\eta\sigma}=0, \quad f_{\eta\eta\sigma}=1 \quad \text{for the boundary-layer case} \tag{13a}$$

$$\text{or} \quad f_{\eta\sigma}=1, \quad f_{\eta\eta\sigma}=0 \quad \text{for the wake flow}$$

$$\text{at} \quad \eta=\eta_{\text{edge}} \qquad f_{\eta\sigma}=f_{\eta\eta\sigma}=0 \tag{13b}$$

Note that the complete set of equations is linear, requiring a single inversion to obtain the derivatives $(f_\sigma)_j$, $(f_{\eta\sigma})_j$, $(f_{\eta\eta\sigma})_j$, and $(f_{\eta\eta\eta\sigma})_j$ for all $j=1, N$ and the perturbation of the longitudinal pressure gradient β_σ. Once β_σ is computed, one can easily evaluate $\partial u_e/\partial\sigma$, and the pressure sensitivity function $\partial p/\partial\sigma$ follows. The correction of the assumed boundary conditions is then obtained from Eq. (10), and all variables are updated. This process is repeated until the desired pressure is obtained. This procedure can be considered to be a classical optimization technique driving (p^m-p^0) to zero.

Method of Solution

The problem of a two-dimensional viscous flow undergoing separation can be divided into three streamwise zones: 1) the preseparation region, 2) the separation bubble, and 3) the

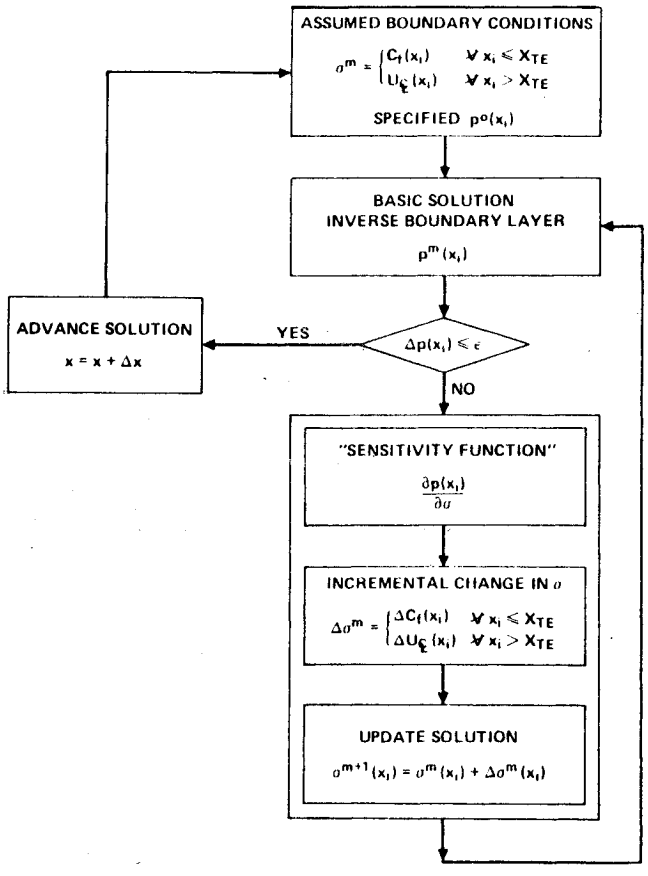

Fig. 2 Solution procedure for attached flow.

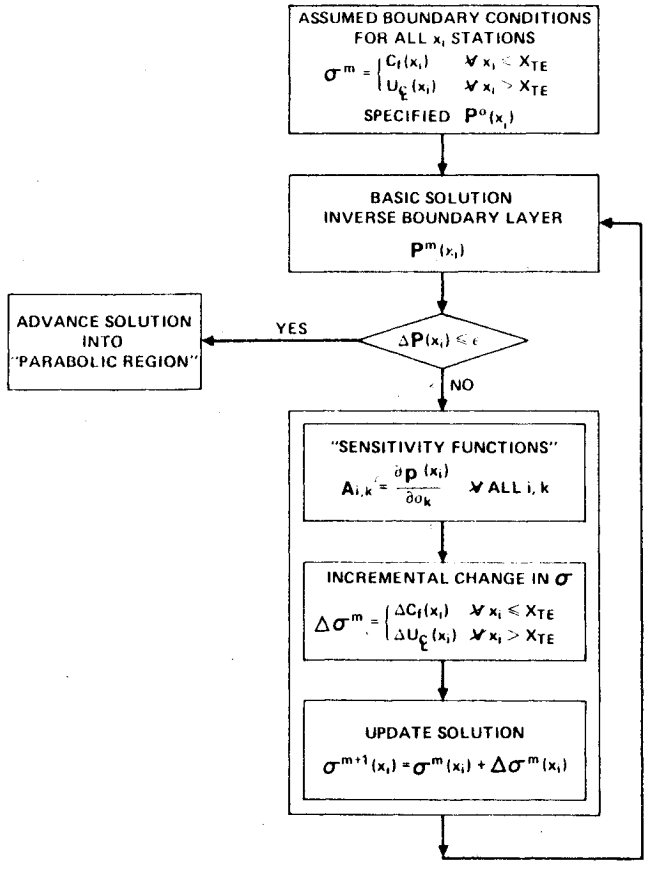

Fig. 3 Solution procedure for separated flow.

post-reattachment region. This structure is convenient to describe the different types of solutions and the way the sensitivity function is evaluated. In the preseparation region the problem is strictly parabolic, so that the iterations on the boundary conditions, if necessary, may be performed locally while marching downstream. In the separation bubble the problem is weakly elliptic, i.e., the upstream effects are small but not negligible; therefore, an iterative sweeping process must be used to account for these upstream influences. Also, the evaluation of the sensitivity functions is affected by this elliptic nature. In the post-reattachment zone, the problem is again parabolic and, therefore, suitable for simple local iteration.

Parabolic Region

Flow regions with negligible upstream influence like the preseparation boundary-layer flow, the post-reattachment boundary layer, or the wake flow are referred to as "parabolic regions." Usually when solving such flows the pressure distribution $p^0(x)$ along the surface is known. If an inverse mode calculation is elected, an additional boundary condition is specified $C_f(x)$ for boundary layers or $u_{\ell}(x_i)$ for wakes to replace the pressure gradient $\beta(x_i)$ at the particular streamwise station x_i.

For the preseparation region, the inverse mode must be invoked some distance upstream of the separation point in order to avoid singular behavior. Figure 2 schematically describes the numerical procedure. The basic solution of the equations with the prescribed boundary condition will converge to the external quantities $p^m(x_i)$, $u_e^m(x_i)$, and $\beta^m(x_i)$ that are different from the desired $p^0(x_i)$, $u_e^0(x_i)$, $\beta^0(x_i)$, respectively. In this case, the solution enters the optimization loop computing the amount of change in σ needed to obtain the prescribed $p^0(x_i)$. Once this value is reached, the computation can be advanced to the next streamwise station. For cases considered here, three or four iterations of the entire loop are required.

Elliptic Region

The case for solving the flow in a separated bubble is somewhat different. The "ellipticity" of the flow causes each x station to be affected by any change in any of the other stations. To account for this tight coupling, influence coefficients are introduced. The procedure for solving this elliptic region is illustrated in Fig. 3. The expansion of the pressure distribution $p(x)$ in terms of σ [Eq. (9)] can be rewritten to first order as

$$p^{m+1}(x_i) = p^m(x_i) + \sum_{k=1}^{K} \frac{\partial p(x_i)}{\partial \sigma_k} \Delta\sigma_k \tag{14}$$

where $\partial p(x_i)/\partial \sigma_k$ may be interpreted as the sensitivity of the pressure at station x_i with respect to a change in the boundary condition at station x_k, and K is the number of streamwise stations in the bubble. This relation can be written in a matrix form

$$\bar{A} \cdot \Delta\bar{\sigma} \cong \Delta\bar{P} \tag{15}$$

where $\bar{A}$ is a square $(K \times K)$ matrix containing all of the sensitivity derivatives, $\Delta\bar{\sigma}$ is the correction vector of the boundary conditions of length (K), and $\Delta\bar{P}$ is a vector containing the K differences between the computed pressure distribution and the desired one. The correction of the boundary conditions required for the complete bubble is given by

$$\Delta\bar{\sigma} = \bar{A}^{-1} \cdot \Delta\bar{P} \tag{16}$$

Equation (14) is simply the K dimensional generalization of Eq. (9). The upstream boundary of this region is determined by inverse boundary-layer solution in the parabolic region, while the downstream boundary is free to float.

It should be noted here that the influence matrix $\bar{A}$ is obtained by solving a system of $(4N-4)$ linear equations [Eqs.

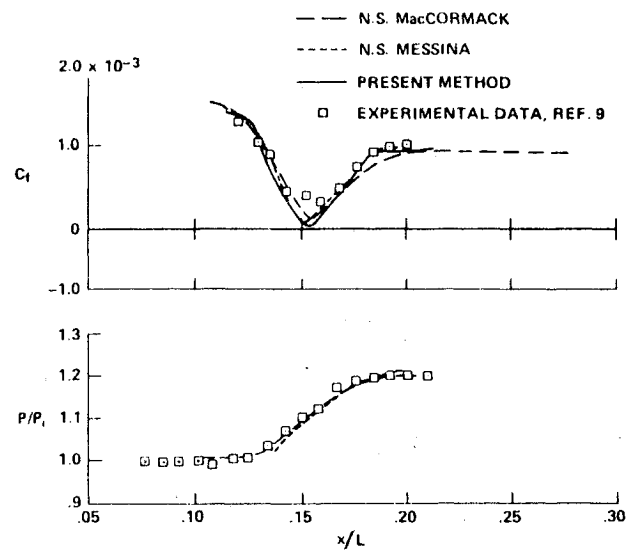

Fig. 4 Comparison of several predictions with experimental data for an unseparated boundary-layer/shock-wave interaction.

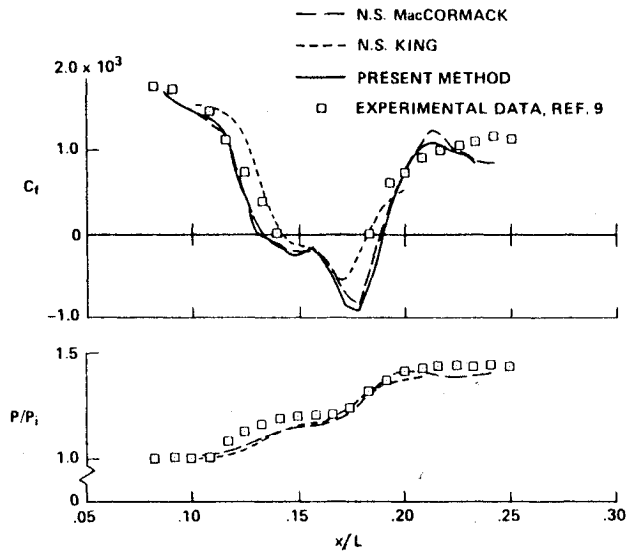

Fig. 5 Comparison of several predictions with experimental data for a separated boundary-layer/shock-wave interaction.

(11) and (12)] K^2 times. After the adjustment of $\bar{\sigma}_k$ $(k=1, K)$ and the updating of all the dependent variables, the basic solution is repeated to check the agreement between the computed pressure and the prescribed one. For the cases run thus far, two or three iterations are required to converge to the prescribed pressure distribution $(p(x)/p_0)$ within 0.0005. When convergence is obtained, the calculation is advanced downstream, entering the "parabolic region" of the post-reattachment zone again.

Results

The present method has been applied to two classes of flows—a supersonic flow involving the interaction of a laminar boundary layer and an oblique shock wave on a flat plate, and a transonic flow over a NACA 64A010 airfoil. Although the laminar boundary-layer, shock-wave interaction is not particularly interesting from a practical point of view, it has become a standard test case for methods which purport to treat flows having strong viscous-inviscid interaction. As a result, a large body of computational results exists for comparison purposes.

Two different laminar boundary-layer, shock-wave interaction flows will be considered: one, where the boundary layer is attached throughout the interaction, and another, where the boundary layer separates in the interaction. Surface-pressure and skin-friction distributions for the attached case are shown in Fig. 4. The experimental data are those of Hakkinen et al.[9] Two different Navier-Stokes solutions[10,11] and the present method are compared with the experimental data. It should be noted that the solution labeled "MacCormack" (Fig. 4) is not, in fact, that reported in Ref. 11, but rather a recalculation using MacCormack's code of those results on a much finer mesh. Both Navier-Stokes solutions (Fig. 4) yield surface-pressure and skin-friction distributions which agree with one another, as well as with the experimental surface-pressure distribution. Further, when the MacCormack surface-pressure distribution is input into the present method, a skin-friction distribution that agrees well with the MacCormack prediction is obtained. All of the calculations tend to predict a skin-friction distribution that is lower than the experimental value in the vicinity of the minimum of that quantity. This disagreement is due to the experimental technique used to obtain skin friction—a Preston tube calibrated in a zero pressure-gradient flow.[9] Under such circumstances the Preston tube yields high values of skin friction in an adverse pressure gradient and low values in a favorable pressure gradient. In the adverse pressure

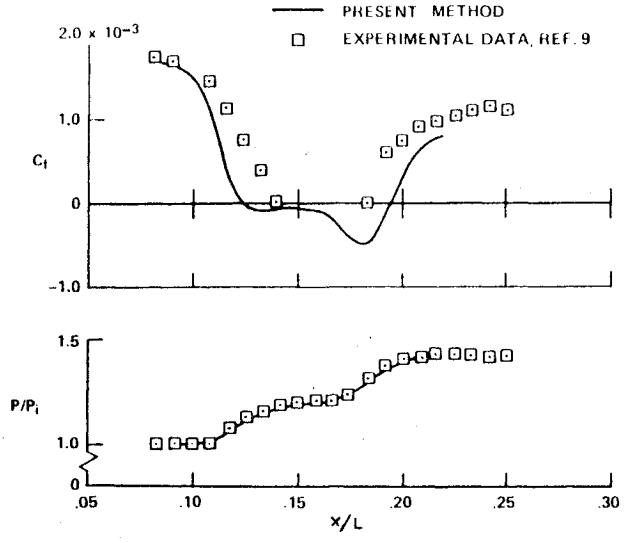

Fig. 6 Comparison of the present method with experimental data for a separated boundary-layer/shock-wave interaction using the experimental pressure distribution.

gradient of this flow, the Preston tube would be expected to predict a skin friction higher than the true value. This is one of the very few cases where the authors believe the calculations to be more accurate than the experiment.

Surface-pressure and skin-friction distributions for the separated case are shown in Fig. 5. The experimental data again are due to Hakkinen et al. (see Fig. 6b of Ref. 9). Again, two different Navier-Stokes solutions[11,12] and the present method are compared with the experimental data. For this case, both Navier-Stokes solutions produce nearly the same pressure distribution, but differ somewhat in their predicted skin-friction distributions. Again, it should be noted that the MacCormack solution is a recalculation of the results of Ref. 11 on a much finer mesh. When the MacCormack pressure distribution is input into the present method, a skin-friction distribution that agrees well with the MacCormack prediction is obtained. A disturbing feature of these comparisons is the apparent ability to predict the skin-friction distribution, at least insofar as defining the limits of the separation bubble. Yet the methods fail to predict the experimentally observed surface-pressure distribution, particularly upstream of the shock impingement. This is all the more puzzling in light of

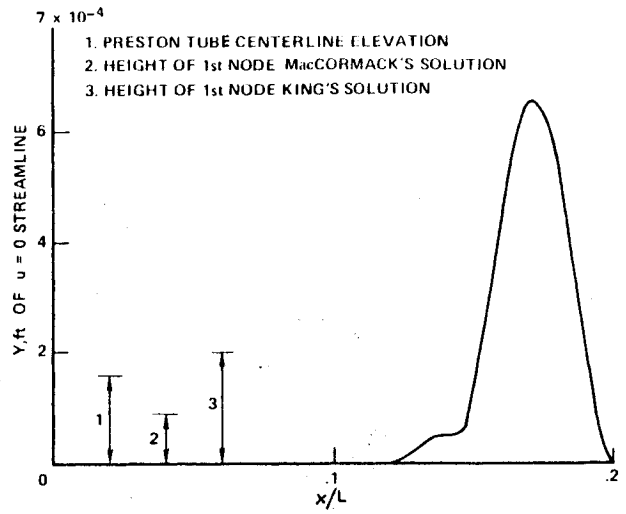

Fig. 7 Comparison of locus of $u=0$ points from solution of Fig. 6 with nodal configuration of Navier-Stokes and Preston tube height.

the aforementioned inaccuracy of the Preston tube in measuring skin friction in an adverse pressure gradient and the accuracy with which surface static pressures can be determined. This behavior, however, is characteristic of all the Navier-Stokes solutions for this case with which the authors are familiar.

In order to investigate this discrepancy, the experimental pressure distribution was input into the present method. The intent was to determine a skin-friction distribution consistent with that pressure distribution within the framework of the present theory. As can be seen in Fig. 6, the resulting separation point is substantially upstream of the experimental value and those indicated by the Navier-Stokes solutions. If experimental pressure distribution were assumed to be correct (a reasonable assumption in light of the ease of measuring surface pressure relative to measuring skin friction), then the Navier-Stokes solutions would be in error. It should be noted that the extent of the separation bubble from the present prediction is in good agreement with the physically based free-interaction boundary-layer solutions of Ref. 13.

In view of this situation, several questions must be answered:

1) Why do the Navier-Stokes solutions agree with the skin-friction distribution for the separated flow?

2) Why do these same solutions disagree with the pressure distribution for the separated flow?

3) Why do all high resolution solutions agree with each other and with the experimental surface pressure data for the attached flow and not for the separated flow?

A consistent argument can be proposed based on the configuration of the zero velocity line. Figure 7 shows the locus of the points characterized by $u=0$, with the elevation of the Preston tube centerline and the distance from the wall to the first node in each of the two Navier-Stokes solutions. It is clear that the smallest scale resolvable by any method, experimental or numerical can be no smaller than the smallest scale associated with the method in question. In the case of the experimental measurement, this scale is the elevation of the Preston tube centerline, while in the numerical methods this scale is the local nodal spacing. If the intersection of each of these elevations with the $u=0$ locus were taken to define separation, the MacCormack solution should predict separation somewhat upstream of the measured value, and the King solution somewhat downstream of the measured value, consistent with the results shown in Fig. 5. In addition, it is clear that neither the Navier-Stokes solutions nor the Preston tube can resolve the upstream tail of the separation bubble, and the upstream displacement effect which produces the pressure rise cannot be resolved.

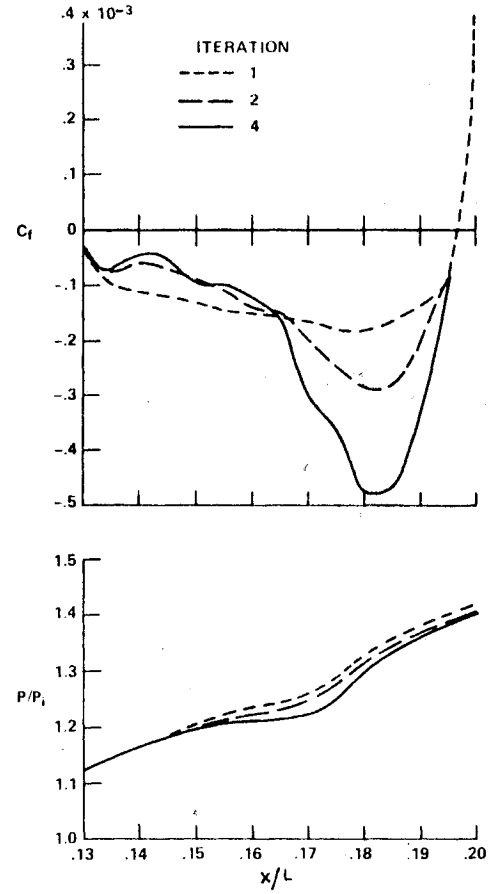

Fig. 8 Iteration history for solution of Fig. 6.

We can now address the previously stated questions.

1) The Navier-Stokes equations agree with the experimental skin-friction distribution because the smallest resolvable scales for both are comparable.

2) The Navier-Stokes solutions do not agree with the experimental pressure distribution because they cannot resolve the upstream tail of the separation bubble. Due to this lack of resolution, part of the displacement effect ahead of shock impingement was missed.

3) All the methods agree for the unseparated case because for this case, there are no relevant physical scales in the flow which are smaller than the Navier-Stokes mesh.

The preceding observations appear to be consistent with all the facts, but a definitive resolution of the problem will require a Navier-Stokes solution for the Hakkinen[9] case, with a Δy in the wall region of the order of 10^{-5} ft, about 1/10 the Δy of the Navier-Stokes solution shown in Fig. 5.

The authors made an effort to resolve this question by mesh refinement, using the fast MacCormack algorithm.[14] It was found that the simple introduction of additional nodal points near the wall caused strongly aphysical behavior, apparently due to the loss of accuracy introduced by the rapid increase in Δy away from the wall. Uniform mesh reduction was limited by machine core storage and computational cost to 28 points in the fine mesh and, although some variation of the solutions was apparent, no consistent trends were observed.

Figure 8 shows the iteration history for the present method for the solution shown in Fig. 7. For this case, four iterations were required to force the computed pressure vector to be everywhere within 10^{-3} of the input pressure vector.

The conclusions to be drawn from the foregoing are: 1) for slender separation bubbles at moderate Mach numbers, the boundary-layer equations contain all of the relevant physics; 2) the present method, which is fourth-order accurate in the y direction with a mesh of typically 20-25 points in the boun-

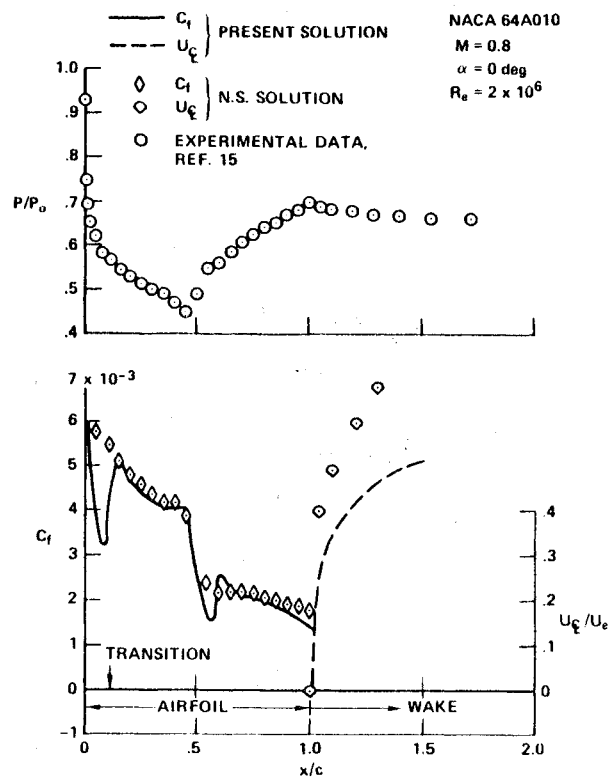

Fig. 9 Comparison of present method with Navier-Stokes solution for flow of a transonic airfoil.

dary layer, provides substantially better resolution of the viscous flow than is practically possible with second-order accurate Navier-Stokes codes; and 3) the advantages of modeling such flows with the Navier-Stokes solutions are open to question in light of the development of this new method. In addition, if one is concerned with either the interpretation of experimental data or with turbulence modeling, the present method might prove extremely useful since the experimental pressure distribution may be imposed on the calculation.

Having established the numerical and physical accuracy and the utility of the present method, we turn our attention to a problem of more practical importance, i.e., transonic flow over a 64A010 airfoil. Figure 9 shows the experimental pressure distribution with predicted skin-friction distribution on the airfoil and the wake centerline velocity downstream of the airfoil. For this unseparated case for which $M=0.8$, $\alpha=0$, $Re_c=2\times10^6$, the surface pressure as obtained from the experiment of Ref. 15, inviscid calculations, and Navier-Stokes calculations are essentially in agreement. The skin-friction distribution and wake centerline velocity as obtained from Deiwert's code[16] and the present method are compared in the lower portion of the figure. The large discrepancy in C_f near the leading edge is caused by the fact that the present method was run in the laminar mode up to the location of the transition strip with instantaneous transition to turbulence at that point. Quite reasonable agreement is found between the Navier-Stokes solution and the present method for skin-friction coefficients on the airfoil and rather poor agreement in centerline velocity in the wake.

Figure 10 compares a measured and predicted velocity distribution and turbulent shear-stress distribution 2% of the chord aft of the trailing edge. The experimental values are those of Johnson.[15] The predicted values were obtained using Deiwert's code (as presented in Ref. 15) as well as the present method. It can be seen that the present method, using a simple mixing-length turbulence model, provides a reasonably good prediction of both velocity and turbulent shear stress. The relatively poor performance of the Navier-Stokes calculations

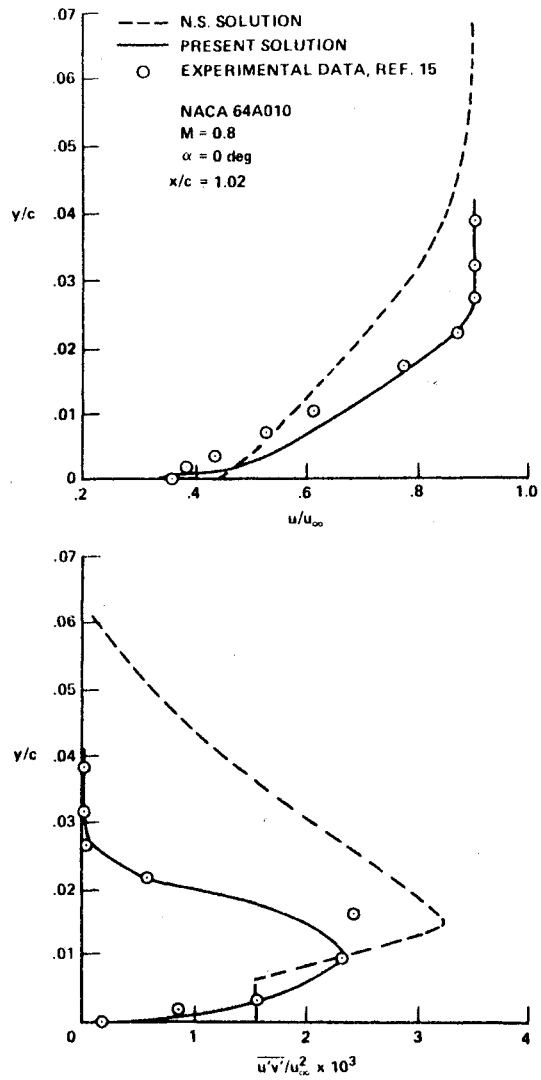

Fig. 10 Comparison of present method with Navier-Stokes solution and experimental data flow in the near wake of a transonic airfoil.

for this case is attributed to inadequate resolution of the boundary layer in the computational mesh. However, the comparison of Figs. 9 and 10 raises a fundamental question: "If the boundary layer were well resolved in the calculations of the present method and poorly resolved in the Navier-Stokes calculation, why do the skin-friction distributions obtained by the two methods appear to agree so well?" An examination of the two solutions indicates that in the wall region, the velocity gradients in the Navier-Stokes solution are about half of those obtained from the present method, while the effective viscosity is about twice that of the present method. The agreement between the two solutions must, therefore, be regarded as fortuitous.

Figure 11 presents the experimental pressure distribution[15] imposed on the present method with the predicted skin-friction distribution for the 64A010 airfoil at 6.2 deg incidence, for which catastrophic separation occurs at the shock wave. Although a Navier-Stokes solution was run for this case, it is not presented because of large uncertainties associated with tunnel-wall corrections invoked in the calculations. As a result, the predicted pressure in the Navier-Stokes calculation only vaguely resembles the experiment. Insofar as the skin-friction distribution predicted by the present method is concerned, we have reasonable confidence in the predicted values from the leading edge to the separation point. Downstream of separation, these values are too high due to inadequacies in the zero equation turbulence model used.[17]

Table 1 CDC 7600 CPU time for the presented calculations

Case study	Source of pressure distribution data	Total number of x stations	Number of stations in the bubble	CDC 7600 CPU time, s
Hakkinen 6a	Experiment	32	0	4
Hakkinen 6b	Navier-Stokes solution	32	10	27
Hakkinen 6b	Experiment	32	14	39
NACA 64A010 $\alpha = 0$ deg	Experiment/inviscid Navier-Stokes	32	0	3
NACA 64A010 $\alpha = 6.2$ deg	Experiment	32	4	6

The efficiency of the present method may be evaluated by considering the 7600 CPU times given in Table 1 for the flows considered here. (Note that the machine time required for solution is a function of the accuracy of the assumed skin-friction distribution and the number of streamwise stations within the separated region.)

The success of the method to date brings up some interesting mathematical questions regarding uniqueness of the solutions obtained. The authors are not prepared, at present, to offer rigorous demonstrations of uniqueness, but our experience to date with the method indicates that the only parameter subject to the goodness of the first guess is the rate of convergence. This is subject to two conditions: 1) the inverse method must be "turned on" upstream of the separation point, indicated by the first guess of C_f, and 2) the separation point of the first guess must be selected to occur upstream of any separation point ultimately predicted. This latter condition could be eliminated at the cost of some additional program logic.

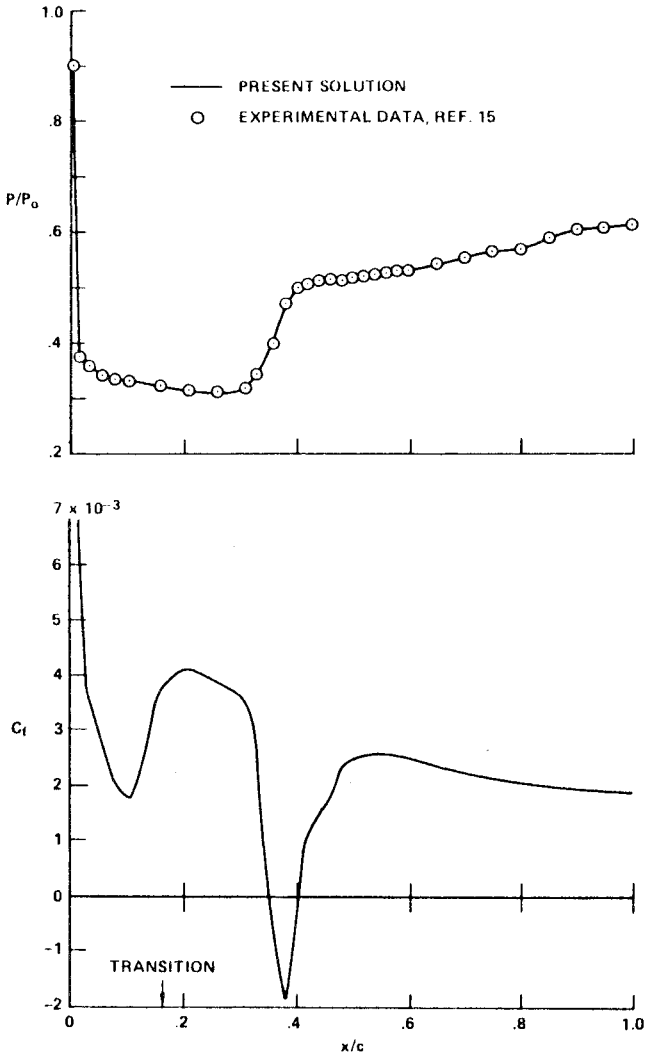

Fig. 11 Solution of the present method for flow over a transonic airfoil at 6.2 deg angle of attack.

Concluding Remarks

It has been shown that the present method can reproduce the essential features of the full Navier-Stokes solutions if a pressure distribution is supplied. The obvious applications of the method are: 1) in conjunction with an inviscid code, to produce complete flowfield solutions with no ab-initio knowledge of the pressure distribution; 2) to optimize turbulence models by comparison with experimental data for flows with very strong adverse pressure gradients; and 3) to aid in wind-tunnel data interpretation for transonic flows in which the correct far-field boundary conditions, required by Navier-Stokes solutions, are unknown due to wall-interference effects.

In the case of coupling the present method to an inviscid outer calculation through a viscous-inviscid interaction procedure, the present scheme would, conceptually, closely approach that of Carter.[18] It is anticipated that the fourth-order accuracy of the present method with its rather sparse nodal array requirements might permit more efficient computation for the same accuracy.

We should make clear that the present method is still a boundary-layer method. Despite the fact that we have overcome the separation-point singularity problem, the method is applicable only to flows with relatively slender separation bubbles, for which the basic assumption $v/u \ll 1$ remains valid.

Finally, it is clear that solutions to the Navier-Stokes equations, presented in the literature up to this time, should be re-examined in the light of the very fine mesh spacing which may be required to resolve physically relevant features of the flow.

References

[1] Klineberg, J. M. and Steger, J. L., "The Numerical Calculation of Laminar Boundary Layer Separation," NASA TN D-7732, July 1974.

[2] Carter, J. E. and Wornom, S. F., "Solutions for Incompressible Separated Boundary Layers Including Viscous-Inviscid Interaction in Aerodynamic Analysis Requiring Advanced Computers," NASA SP 347, 1975, pp. 125-150.

[3] Murphy, J. D., Presley, L. K., and Rose, W. C., "On the Calculation of Supersonic Separating and Reattaching Flow," AGARD Conference on Flow Separation, AGARD CP 168, Paper 22, 1975.

[4] Peyret, R. and Viviand, H., "Computation of Viscous Compressible Flows Based on the Navier-Stokes Equations," AGARD-AG-212, Paris, 1975.

[5] Murphy, J. D., "Application of the Generalized Galerkin Method to the Computation of Fluid Flows," *Proceedings of the AIAA Computational Fluid Dynamics Conference*, Palm Springs, Calif., July 19-20, 1973, pp. 63-68.

[6] Kendall, R. M. and Bartlett, E. P., "Non-Similar Solutions of the Multicomponent Laminar Boundary Layer by an Integral Matrix Method," AIAA Paper 67-218, 1967.

[7] Nachtsheim, P. R. and Swigert, P., "Satisfaction of Asymptotic Boundary Conditions in Numerical Solutions of Boundary-Layer Type," NASA TN D-3004, Oct. 1965.

[8] Rubbert, P. E. and Landahl, M. T., "Solution of the Transonic Airfoil Problem Through Parametric Differentiation," *AIAA Journal*, Vol. 5, March 1967, pp. 470-479.

[9] Hakkinen, R. J., Greber, I., Trilling, L., and Abarbanel, S. S., "The Interaction of an Oblique Shock Wave with a Laminar Boundary Layer," NASA MEMO 2-18-59W, 1959.

[10] Messina, N. A., "A Computational Investigation of Shock Waves, Laminar Boundary Layers and Their Mutual Interaction," Ph.D. Thesis, Princeton University, Princeton, N.J., 1977.

[11] MacCormack, R. W. and Boldwin, B. S., "A Numerical Method for Solving the Navier-Stokes Equations with Application to Shock Boundary-Layer Interactions," AIAA Paper 75-1, San Diego, Calif., 1975.

[12] King, L. S., private communication, NASA Ames Research Center, Nov. 1978.

[13] Murphy, J. D., "A Critical Evaluation of Analytic Methods for Predicting Laminar Boundary-Layer Shock-Wave Interaction," NASA TN D-7044, 1971.

[14] MacCormack, R. W., "An Efficient Explicit-Implicit-Characteristic Method for Solving the Compressible Navier-Stokes Equations," *SIAM-AMS Proceedings*, Vol. II, 1978, pp. 130-155.

[15] Johnson, D. A. and Bachalo, W. D., "Transonic Flow About a Two-Dimensional Airfoil—Inviscid and Turbulent Flow Properties," AIAA Paper 78-1117, Seattle, Wash., 1978.

[16] Deiwert, G. S., "Computation of Separated Transonic Turbulent Flows," *AIAA Journal*, Vol. 14, June 1976, pp. 735-740.

[17] Rose, W. C. and Seginer, A., "Calculation of Transonic Flow Over Supercritical Airfoil Sections," AIAA Paper 77-681, Albuquerque, N. Mex., 1977.

[18] Carter, J. E., "A New Boundary-Layer Interaction Technique for Separated Flows," NASA TM 78690, 1978.